Multiscale Models for Vertebrate Limb Development

Stuart A. Newman,[1] Scott Christley[2,3], Tilmann Glimm[4], H.G.E. Hentschel[5], Bogdan Kazmierczak[6], Yong-Tao Zhang[3,7], Jianfeng Zhu[7] and Mark Alber[3,7]**

[1]Department of Cell Biology and Anatomy, New York Medical College, Valhalla, 10595

[2]Department Computer Science, University of Notre Dame, Notre Dame, IN 46556

[3]Interdisciplinary Center for the Study of Biocomplexity, University of Notre Dame, Notre Dame, IN 46556

[4]Department of Mathematics, Western Washington University, Bellingham, WA 98225

[5]Department of Physics, Emory University, Atlanta, GA 30322

[6]Polish Academy of Sciences, Institute of Fundamental Technological Research, 00-049 Warszawa, Poland

[7]Department of Mathematics, University of Notre Dame, Notre Dame, IN 46556

*Authors for correspondence

Dynamical systems in which geometrically extended model cells produce and interact with diffusible (morphogen) and non-diffusible (extracellular matrix) chemical fields have proved very useful as models for developmental processes. The embryonic vertebrate limb is an apt system for such mathematical and computational modeling since it has been the subject of hundreds of experimental studies, and its normal and variant morphologies and spatiotemporal organization of expressed genes are well-known. Because of its stereotypical proximodistally generated increase in the number of parallel skeletal elements, the limb lends itself to being modeled by Turing-type systems which are capable of producing periodic, or quasi-periodic, arrangements of spot- and stripe-like elements. This chapter describes several such models, including (i) a system of partial differential equations in which changing cell density enters into the dynamics explicitly, (ii) a model for morphogen dynamics alone, derived from the latter system in the "morphostatic limit" where cell movement relaxes on a much slower time-scale than diffusible molecules, (iii) a discrete stochastic model for the simplified pattern formation that occurs when limb cells are placed in planar culture, and (iv) several hybrid models in which continuum morphogen systems interact with cells represented as energy-minimizing mesoscopic entities. Progress in devising computational methods for handling 3D, multiscale, multi-model simulations of organogenesis is discussed, as well as for simulating reaction-diffusion dynamics in domains of irregular shape.

I. Introduction

The vertebrate limb, an array of jointed skeletal elements and associated tissues that arose in fish-like ancestors nearly 400 million years ago, has long held central importance in the fields of developmental and evolutionary biology (reviewed in Newman and Müller, 2005). The developing limb is relatively easy to manipulate surgically in the embryos of avian species such as the chicken. In mammals, such as the human and mouse, it is subject to mutations of large effect that do not otherwise prove fatal to the organism. In fish and amphibians the paired limbs, or related structures, exist with variant anatomical characteristics and regenerative properties. And limb mesenchymal cells can be grown in culture, where they undergo differentiation and pattern formation with a time-course and on a spatial scale similar to that in the embryo. The limb is therefore an ideal system for studying developmental dynamics, genetics, origination and plasticity of multicellular form. Over the last 60 years, knowledge of the tissue, cellular, and molecular interactions involved in generating a vertebrate limb has accumulated dramatically based on the incisive application of new technologies to all of these systems.

The products of scores of genes have been found to participate in limb development (reviewed in Tickle, 2003) and many of these are impaired by mutation or exogenous substances. But genes and their interactions are neither an exclusive nor exhaustive explanatory level for developmental change (Newman, 2002). The physics of viscoelastic materials and excitable media, *i.e.*, mesoscopic matter, must also enter into the molding and patterning of tissues (Forgacs and Newman, 2005). In particular, they will contribute to the set of dynamic processes by which the interactions of limb bud cells with their various intra- and extracellular molecular components, result in a series of

articulated, well-arranged rods and nodules of cartilage, and later, bone (Newman and Frisch, 1979).

As with many complex, multiscale, phenomena in biology, insight into emergent organizational properties can be gained by, and indeed require, mathematical and computational modeling. Such modeling does not replace analysis at the cellular and molecular levels, but complements it. Mathematics and computational analysis are the best means we have for describing and understanding the spatiotemporal behaviors of systems containing many components, operating on multiple scales.

Developing organs have both discrete and continuous aspects; they may undergo changes according to deterministic or stochastic rules. Some embryonic tissues are planar and can be approximated as 2D sheets, whereas other tissues are space-filling and inherently 3D. Some developmental processes are synchronized over a spatial domain whereas others sweep across a region over time. Some changes occur autonomously within a given tissue type, while others only proceed by unidirectional or reciprocal interactions between pairs of tissues. In some cases, one developmental process will relax much faster or much slower than another, so that the two can be treated essentially independently of one another. In other cases, the only accurate representation is to treat the processes as mutually determinative and conditioning. Each of these possibilities presents a distinct problem for the modeler, and it is becoming increasingly clear that a fully satisfactory model for the development of any living organ must embody all of them. That is, it will be inescapably hybrid, mathematically and computationally.

This article presents several approaches taken by ourselves and others to modeling skeletal pattern formation during development of the vertebrate limb. Because of the

constraints and technical difficulties of producing a multiscale, 3D, hybrid model, as well as the incompleteness of our knowledge of the relevant molecules and the topology, relative strengths and rates of their interactions, the models presented are partial and provisional. Nonetheless, the shortcomings of each of the component models and modeling attempts are usually quite obvious, and we also report on work in progress to remedy them in pursuit of increasingly realistic explanatory accounts.

II. Tissue Interactions and Gene Networks of Limb Development

The limb buds of vertebrates emerge from the body wall, or flank, at four discrete sites – two for the forelimbs and two for the hindlimbs. The paddle-shaped limb bud mesoblast, which gives rise to the skeleton and muscles, is surrounded by a layer of simple epithelium, the ectoderm. The skeletons of most vertebrate limbs develop as a series of precartilage primordia in a *proximodistal* fashion: that is, the structures closest to the body form first, followed, successively, by structures more and more distant from the body. For the forelimb of the chicken, for example, this means the humerus of the upper arm is generated first, followed by the radius and ulna of the mid-arm, the wrist bones, and finally the digits (Saunders, 1948; reviewed in Newman, 1988) (Fig. 1). Urodele salamanders appear to be an exception to this proximodistal progression (Franssen *et al.*, 2005). Cartilage is mostly replaced by bone in species with bony skeletons.

Before the cartilages of the limb skeleton form, the mesenchymal cells of the mesoblast are dispersed in a hydrated ECM, rich in the glycosaminoglycan hyaluronan. The first morphological evidence that cartilage will differentiate at a particular site in the

mesoblast is the emergence of precartilage mesenchymal condensations. The cells at these sites then progress to fully differentiated cartilage elements by switching their transcriptional capabilities. Condensation involves the transient aggregation of cells within a mesenchymal tissue. This process is mediated first by the local production and secretion of ECM glycoproteins, in particular, fibronectin, which act to alter the movement of the cells and trap them in specific places. The aggregates are then consolidated by direct cell-cell adhesion. For this to occur the condensing cells need to express, at least temporarily, adhesion molecules such as N-CAM, N-cadherin, and possibly cadherin-11 (reviewed in Hall and Miyake, 1995; 2000; Forgacs and Newman, 2005).

Because all the precartilage cells of the limb mesoblast are capable of producing fibronectin and cadherins, but only those at sites destined to form skeletal elements do so, there clearly must be communication among the cells to divide the labor in this respect. This is mediated in part by secreted, diffusible factors of the TGF-β family of growth factors, which promote the production of fibronectin (Leonard *et al.*, 1991). Limb bud mesenchyme also shares with many other connective tissues the autoregulatory capability of producing more TGF-β upon stimulation with this factor (Miura and Shiota, 2000; Van Obberghen-Schilling, *et al.*, 1988).

The limb bud ectoderm performs several important functions. First, it is a source of fibroblast growth factors (FGFs) (Martin, 1998). Although the entire limb ectoderm produces FGFs, the particular mixture produced by the apical ectodermal ridge (AER), a narrow band of specialized ectodermal cells running in the anteroposterior direction along the tip of the growing limb bud in birds and mammals, is essential to limb

outgrowth and pattern formation. FGF8 is the most important of these (Mariani and Martin, 2003). It is expressed mainly in the AER in amniotes (birds and mammals), but is also expressed in limb bud mesenchyme in urodeles (Han *et al.*, 2001). The AER affects cell survival (Dudley *et al.*, 2002) and keeps the precondensed mesenchyme of the "apical zone" in a labile state (Kosher *et al.*, 1979). Its removal leads to terminal truncations of the skeleton (Saunders, 1948).

The FGFs produced by the ectoderm affect the developing limb tissues through one of three distinct FGF receptors. The apical zone is the only region of the mesoblast-containing cells that expresses FGF receptor 1 (FGFR1) (Peters *et al.*, 1992; Szebenyi *et al.*, 1995). In the developing chicken limb, cells begin to condense at a distance of approximately 0.3 mm from the AER. In this zone FGFR1 is downregulated and cells that express FGFR2 appear at the sites of incipient condensation (Peters *et al.*, 1992; Szebenyi *et al.*, 1995; Moftah *et al.*, 2002). Activation of these FGFR2-expressing cells by FGFs releases a laterally-acting (that is, peripheral to the condensations) inhibitor of cartilage differentiation (Moftah *et al.*, 2002). Although the molecular identity of this inhibitor is unknown, its behavior is consistent with that of a diffusible molecule, or one whose signaling effects propagate laterally in an analogous fashion. Recent work suggests that Notch signaling also plays a part in this lateral inhibitory effect (Fujimaki *et al.*, 2006). The roles of TGF-β, the putative lateral inhibitor, and fibronectin in mediating precartilage condensation in the limb bud mesenchyme can be schematized in the form of a "core" cell-molecular-genetic network (Fig. 2).

Finally, differentiated cartilage in the more mature region, proximal to the condensing cells, expresses FGFR3, which is involved in the growth control of this tissue

(Ornitz and Marie, 2002). The ectoderm, by virtue of the FGFs it produces, thus regulates growth and differentiation of the mesenchyme and cartilage.

The limb ectoderm is also involved in shaping the limb bud. By itself, the mesenchyme, being an isotropic tissue with liquid-like properties, would tend to round up (Forgacs and Newman, 2005). Ensheathed by the ectoderm, however, it assumes a paddle shape. This appears to be due to the biomechanical influence of the epithelium, the underlying basal lamina of which is organized differently beneath the dorsoventral surfaces and the anteroposteriorly arranged AER (Newman *et al.*, 1981). There is no entirely adequate biomechanical explanation for the control of limb bud shape by the ectoderm (but see Dillon and Othmer, 1999 and Borkhvardt, 2000, for suggestions).

III. Models for Chondrogenic Pattern Formation

A. Limb Mesenchyme as a "Reactor-Diffusion" System

Reaction-diffusion systems, in which a particular network of positive and negative feedbacks in the production, and disparate diffusion rates, of molecular species, have attracted interest as biological pattern-forming mechanisms ever since their well-known proposal as the "chemical basis of morphogenesis" by A. M. Turing half a century ago (Turing, 1952). Experimentally motivated reaction-diffusion-type models (not all of them conforming to Turing's precise scheme) have been gaining prominence in many areas of developmental biology (Forgacs and Newman, 2005; Maini *et al.*, 2006), including the patterning of the pigmentation of animal skin (Yamaguchi *et al.*, 2007), feather germs (Jiang *et al.*, 2004), hair follicles (Sick *et al.*, 2006), and teeth (Salazar-Ciudad and Jernvall, 2002). As we have seen, patterning of the limb skeleton is dependent on molecules of the TGF-β and FGF classes, which are demonstrably

diffusible morphogens (Lander *et al.*, 2002; Williams *et al.*, 2004; Filion and Poper, 2004). Like reaction-diffusion systems, moreover, the developing limb has self-organizing pattern-forming capability. It is well-known, for example, that many transcription factors (*e.g.*, the Hox proteins) and extracellular factors (*e.g.*, Sonic hedgehog protein, retinoic acid) are present in spatiotemporal patterns during limb development, and disrupting their distributions leads to skeletal anomalies (Tickle, 2003). Nevertheless, randomized limb mesenchymal cells with disrupted gradients of Hox proteins, Shh, etc., give rise to digit-like structures in vivo (Ros *et al.*, 1994) and discrete, regularly spaced cartilage nodules in vitro (Downie and Newman, 1994; Kiskowski *et al.*, 2004). Moreover, simultaneous knockout of Shh and its inhibitory regulator Gli3 in mice yields limbs with numerous extra digits (Litingtung *et al.*, 2002). If anything, such gradients limit and refine the self-organizing capacity of limb mesenchyme to produce skeletal elements rather than being required for it.

Beyond this, the following experimental findings, count in favor of the relevance of a reaction-diffusion mechanism for limb pattern formation: (i) The pattern of precartilage condensations in limb mesenchyme in vitro changes in a fashion consistent with reaction-diffusion mechanism (and not with an alternative mechanochemical mechanism) when the density of the surrounding matrix is varied (Miura and Shiota, 2000b); (ii) exogenous FGF perturbs the kinetics of condensation formation by limb precartilage mesenchymal cells in vitro in a fashion consistent with a role for this factor in regulating inhibitor production in a reaction-diffusion model (Miura and Maini, 2004); (iii) the "thick-thin'" pattern of digits in the *Doublefoot* mouse mutant can be accounted for by the assumption

of that the normal pattern is governed by a reaction-diffusion process the parameters of which are modified by the mutation (Miura *et al.*, 2006).

The scale-dependence of reaction-diffusion systems (*i.e.*, the addition or loss of pattern elements when the tissue primordium has variable size), sometimes considered to count against such mechanisms for developmental processes, may actually represent the biological reality in the developing limb. Experiments show, for example, that the number of digits that arise is sensitive to the anteroposterior (thumb-to-little finger breadth) of the developing limb bud, and will increase (Cooke and Summerbell, 1981) or decrease (Alberch and Gale, 1983) over typical values if the limb is broadened or narrowed.

B. The Core Patterning Network in a Geometric Setting

The developing limb has a smooth, but non-standard, geometric shape that changes over time. Moreover, different processes take place in different parts of the developing structure. As is the case with somitogenesis along the body axis (Pourquié, 2003; Schnell *et al.* and Baker *et al.*, this volume), the ectoderm at the distal tip of the pattern-forming system (the tail tip and the AER) produces FGFs that keep a zone of tissue within the high end of the gradient in an immature, unpatterned state.

To simplify the presentation of our basic limb development model, we made the following geometric idealization (Newman and Frisch, 1979; Hentschel *et al.*, 2004): the limb bud is considered as a parallelepiped of time-dependent proximodistal length, $L(t)$, taken along the x–axis, and fixed length, l_y, along the anteroposterior (thumb to little finger) direction (y-axis). The dorsoventral (back to front) width (z-axis) was collapsed

to zero in this schematic representation (Fig. 3). The developing limb bud is considered, based on classic observations, to consist of three regions: an "apical zone" of size $l_{\text{apical}}(t)$, at the distal tip of the bud, consisting of non-condensing mesenchymal cells, an "active zone," proximal to the apical zone, of length $l_x(t)$, which contains differentiating and condensing cell types, and a "frozen zone" of length $l_{\text{frozen}}(t)$, containing differentiated cartilage cells, proximal to the active zone. The lengths of these zones add up to that of the entire limb bud: $L(t) = l_{\text{apical}}(t) + l_x(t) + l_{\text{frozen}}(t)$.

The dynamic model we present in the following section resides within, but is not uniquely tied to, the schematic shown in Fig. 3. While the division into apical, active and frozen zones is experimentally motivated and is inherent to our conception of the spatiotemporal organization of limb development, the 2D rectilinear template of Fig. 3 is presented for didactic purposes. Our goal, partly implemented in subsequent sections, is to model the cellular and molecular dynamics in the 3D space of a naturally contoured limb bud.

C. "Bare-Bones" System of Reactor-Diffusion Equations

We refer to the dynamic model for limb development presented here as "bare-bones," because while it incorporates the core mesenchymal cell-morphogen-ECM network summarized in Fig. 2, it omits the spatiotemporal modulatory factors such as Hox protein gradients, Shh, and so on, that cause the various skeletal elements (*e.g.*, the different digits, the radius and ulna) to appear different from one another. As a first pass, we attempt only to model the proximodistal temporal progression of skeletogenesis and the generally increasing number of elements along the proximodistal axis.

As described in earlier sections, limb skeletal patterning involves cycles of cell state changes and local cell movement: mesenchymal cells upregulate their production of fibronectin at particular tissue sites, leading to precartilage condensation. This is followed, in turn, by chondrogenesis (cartilage differentiation). Finally, the spatiotemporal control of these differentiative and morphogenetic changes in the mesenchyme is entirely dependent on products of the surrounding epithelium.

We begin with the hypothesis that the division of the distal portion of the limb into an apical and active zone reflects the activity of the AER in suppressing differentiation of the mesenchyme subjacent to it (Kosher *et al.*, 1979). The spatial relationship between the apical and active zones results from the graded distribution of FGFs, the presumed AER-produced suppressive factors. The active zone, therefore, is where the mesenchyme cells no longer experience high levels of FGFs and therefore become responsive to the activator, TGF-β, and the factors that mediate lateral inhibition. The dynamic interactions of cells and morphogens in the active zone give rise to spatial patterns of condensations. As will be seen, the length of the active zone, $l_x(t)$, serves as a "control parameter" that influences the number of condensations that form.

Cell proliferation enters into this scheme in the following fashion: cells are recruited into the active zone from the proximal end of the apical zone, as dividing cells move away from the influence of the AER. (This is similar to the role of the caudal FGF gradient in somitogenesis; Dubrulle *et al.*, 2001). The active zone loses cells, in turn, to the proximal frozen zone, the region where cartilage differentiation has occurred and a portion of the definitive pattern has become set.

Four main types of mesenchymal cells are involved in chick limb skeletal pattern formation. These are represented in the model by their spatially and temporarily varying densities. The cell types are characterized by their expression of one of the three FGF receptors found in the developing limb. The cells expressing FGFR1, FGFR2 (and cells) and FGFR3 are denoted, respectively, by R_1, $R_2 + R_2^{'}$ and R_3. The apical zone consists of R_1 cells, and those of the frozen zone R_3 cells (reviewed in Ornitz and Marie, 2002). The active zone contains R_2 cells and the direct products of their differentiation, $R_2^{'}$ cells. These latter cells secrete enhanced levels of fibronectin. The R_1, R_2 and $R_2^{'}$ cells are mobile, while the R_3 (cartilage) cells are immobile.

According to our model (Hentschel *et al.*, 2004), transitions and association between the different cell types are regulated by the gene products of the core mechanism (Fig. 2): c, c_a, c_i and ρ denote, respectively, the spatially and temporarily varying concentrations of FGFs (produced by the ectoderm), TGF-β (produced throughout the mesenchyme), a diffusible inhibitor of chondrogenesis produced by R_2 cells, and fibronectin, produced by $R_2^{'}$ cells. The model thus comprises eight variables, with an equation for the behavior of each of them (Eqs. 1-8). These eight variables correspond to the core set of interactions necessary to describe the development of a basic, "bare bones" skeletal pattern (see Fig. 2).

$$\partial c / \partial t = D\nabla^2 c - kc + J(x,t) \quad (1)$$

$$\partial c_a / \partial t = D_a \nabla^2 c_a - k_a c_i c_a + J_a^{1} R_1 + J_a(c_a) R_2 \quad (2)$$

$$\partial c_i / \partial t = D_i \nabla^2 c_i - k_a c_i c_a + J_i(c_a) R_2 \quad (3)$$

$$\partial R_1 / \partial t = D_{cell} \nabla^2 R_1 - \chi div(R_1 \nabla \rho) + r R_1 (R_{eq} - R) + k_{21} R_2 - k_{12}(c, c_a) R_1 \quad (4)$$

$$\partial R_2 / \partial t = D_{cell} \nabla^2 R_2 - \chi div(R_2 \nabla \rho) + r R_2 (R_{eq} - R) + k_{12} R_1 - k_{21} R_2 - k_{22} R_2 \quad (5)$$

$$\partial R'_2/\partial t = D_{cell}\nabla^2 R'_2 - \chi div(R'_2\nabla\rho) + rR'_2(R_{eq} - R) + k_{22}R_2 - k_{23}R'_2 \quad (6)$$

$$\partial R_3/\partial t = r_3 R_3(R_{eq} - R_3) + k_{23}R'_2 \quad (7)$$

$$\partial\rho/\partial t = k_b(R_1 + R_2) + k'_b R'_2 - k_c\rho \quad (8)$$

In this set of equations, R_1, R_2, R'_2 and R_3 are densities of the different kinds of cells and $R = R_1 + R_2 + R'_2$ is the overall density of the mobile cells.

In the simplest formulation, we consider the system's behavior in a smooth (*i.e.*, at least of C^{2+a} class) domain $\Omega \in \mathrm{IR}^n, n \geq 2$, which is assumed to be fixed in space and time, based on the assumption $\tau_m << \tau_g, \tau_d << \tau_g$ (Recall that τ_m, τ_d and τ_g are the characteristic times of morphogen evolution, cell differentiation, and limb growth, respectively.) All of the functions are subject to no-flux boundary conditions

$$\frac{\partial c}{\partial \mathrm{n}} = \frac{\partial c_a}{\partial \mathrm{n}} = \frac{\partial c_i}{\partial \mathrm{n}} = \frac{\partial \rho}{\partial \mathrm{n}} = \frac{\partial R_1}{\partial \mathrm{n}} = \frac{\partial R_2}{\partial \mathrm{n}} = \frac{\partial R'_2}{\partial \mathrm{n}} = \frac{\partial R_3}{\partial \mathrm{n}} = 0 \quad (9)$$

Here n is the outward normal to the spatial domain, so the cells and secreted molecules have zero flux through the boundary.

The variables are intimately interconnected and interacting: diffusing morphogen-type growth factors (*i.e.*, FGFs and TGF-β) and extracellular matrix molecules (*i.e.*, fibronectin) secreted by some cells represent signals for others to move, differentiate or to produce other or more of the same molecules. The interactions among these variables constitute a "reactor-diffusion" system with potential pattern forming capability. We use this term to emphasize that the active component is a living cell, not just a chemical reaction, as in Turing's original formalism.

Simulations using the full system (1-8) are computationally formidable, but we have shown analytically that continuous solutions exist for it (Alber, Hentschel *et al.* 2005).

Along with the initial description of the model we used a biologically motivated separation of time scales to reduce the system to four equations. We have shown the existence of the steady state solutions in the form of stripes and spots in the 2D case and analogous extensions in a 3D case and demonstrated that they cannot be stable at the same time (Alber, Glimm, *et al.* 2005). We then used linear stability analysis to compute solutions on the plane for active zones of progressively decreasing width, arriving at a simulation that accurately portrayed the proximodistal order of appearance and increase in number of skeletal elements in a 2D projection (Hentschel *et al.*, 2004).

Subsequently, using a multiscale, multi-model simulation environment (Izaguirre *et al.*, 2003; Cickovski *et al.*, 2007), we modeled cell rearrangement as an individual-based module in the presence of morphogen fields and cell-state transition rules based on simplifications of system (1)-(8). Although this strategy permitted us to generate 3D simulations with authentic developmental properties (Chaturvedi *et al.*, 2005; Cickovski *et al.*, 2005), the equations for the morphogen dynamics abstracted from the full system (where cell and morphogen changes are interconnected) were fairly ad hoc.

In the next section we describe one attempt to remedy this deficit by deriving an analytically rigorous reduction of the morphogen dynamics to a two-equation system (Alber *et al.*, submitted). To do this we have treated system (1-8) in the biologically plausible "morphostatic limit" (Salazar-Ciudad *et al.*, 2003), *i.e.*, under the assumption that cell differentiation occurs on a faster scale than cell rearrangement.

D. Morphogen Dynamics in the Morphostatic Limit

In this section we consider the bare-bones system for skeletal pattern formation (Eqs. 1-8) in the limiting case in which the dynamics of cell differentiation is faster than

the evolution of the overall cell density. This assumption is consistent with existing experimental evidence, though is not uniquely determined by it. An additional assumption is that the spatial variations in the densities of the various cell types involved are small and can be replaced by a constant density for the analysis of the evolution of the morphogen concentrations.

Rates of limb development vary widely across phylogenetic distances, and it is very unlikely that the characteristic time scales of the various component processes of development all scale proportionally. For this reason, the limit we consider may pertain to limb formation in some species and not others, or only at some stages of limb evolution.

With the above assumptions, system (1)-(8) reduces to two evolution equations for the morphogens (Alber *et al.*, submitted).

$$\frac{\partial c_a}{\partial t} = D_a \nabla^2 c_a + U(c_a) - k_a c_a c_i \tag{10}$$

$$\frac{\partial c_i}{\partial t} = D_i \nabla^2 c_i + V(c_a) - k_a c_a c_i \tag{11}$$

The equations are subject to no-flux boundary conditions. The terms $D_a \nabla^2 c_a$ and $D_i \nabla^2 c_i$ describe diffusion of the morphogens, the term $-k_a c_a c$ represents their decay or inactivation, and the terms $U(c_a)$ and $V(c_a)$ describe their production by cells. Specifically, $U(c_a)$ and $V(c_a)$ are given by

$$U(c_a) = (J_a^1 \alpha(c, c_a) + J_a(c_c)\beta(c, c_a))R_{eq}, \quad V(c_a) = J_i(c_c)\beta(c, c_a)R_{eq}. \tag{12}$$

In these expressions, R_{eq} is the cell density (assumed to be approximately constant, see above), and the terms describing secretion of activator and inhibitor are denoted by J

with appropriate subscripts. Details on the exact form of these terms are given in Alber *et al.*, submitted.

In the classification of developmental pattern forming mechanisms proposed by Salazar-Ciudad and coworkers (Salazar-Ciudad *et al.*, 2003), a "morphostatic" mechanism is one which occurs in two distinct phases: cell interaction that leads to alteration of cell states, and hence changes in pattern, is followed by the action of one of various mechanisms (termed "morphogenetic") which causes spatial rearrangement of cells without changing their states. In contrast, "morphodynamic" mechanisms are ones in which cell state changes and cell rearrangements happen simultaneously. For the limb model we consider here, the morphogenetic process is precartilage mesenchymal condensation.

With reference to the classification of Salazar-Ciudad *et al.* (2003), then, the system (10)-(11) obtained from the assumption that differentiation dynamics relaxes faster than mesenchymal condensation can be considered the "morphostatic limit" of the full (morphodynamic) model of Hentschel *et al.* (2004). Because the relative rates of cell differentiation and cell movement are likely to be subject to natural selection, evolution of morphostatic mechanisms may represent a successful evolutionary strategy in certain cases.

The task of finding parameter ranges under which the system can give rise to patterns (what we refer to as the "Turing space" of the system) is much more tractable in the reduced system (10)-(11) than in the full system (1)-(8). This is due to the smaller number of variables and parameters. In addition, the resulting reduced reaction-diffusion system could then be used in a variety of computational models in which geometries,

additional morphogens and model individual model cells (insofar as they behave according to the assumptions under which the morphogen subsystem was isolated) could be introduced in a controlled fashion. In particular, the fact that the reduced equations are derived from first principles makes them much more appropriate than the ad hoc reaction kinetics used in earlier hybrid continuum-discrete models of the limb (Chaturvedi *et al.*, 2005; Cickovski *et al.*, 2005), and adds to the biological authenticity of these models.

In Alber *et al.* (submitted) the authors considered a broad class of Michaelis-Menten-type kinetics models for the rate terms in (10)-(11). They found that the necessary conditions for the Turing instability are fulfilled across a wide range of parameter values, suggesting that the precise choice of these coefficients does not influence the possibility of the Turing instability. In this sense the system is robust.

For the system (10)-(11) to exhibit a Turing-type instability in the morphostatic limit several constraints on morphogen dynamics must be met. In particular, the results indicate the following qualitative predictions:

1) The maximum production rate of the inhibitor by R_2 cells (*i.e.*, cells bearing FGF receptor 2) exceeds their rate of production of the activator TGF-β.

2) The threshold levels of local TGF-β concentration which elicit maximal production rates by R_2 cells of TGF-β, and of inhibitor, must be of roughly the same order of magnitude.

IV. Simulations of Chondrogenic Pattern Formation

A. Biological Questions Addressed by the Simulations

In this section we introduce several methods to address questions raised by the foregoing biological considerations. While our ultimate objective is to produce a simulation of a vertebrate limb in 3D based solely on biologically authentic cell behaviors, each component of this target hybrid model presents its own computational difficulties, and in most cases neither all of the biological variables nor the parameters of their interactions are available. Below we present a proof-of-principle that biologically authentic chondrogenic patterns can be generated using the postulated cell behaviors and molecular components in a multiscale model. While the system in which this is demonstrated is not the full, growing limb bud, but rather disk-like micromass cultures, which have been studied extensively as an in vitro model for skeletogenesis, it is a system for which detailed quantitative measurements are available. For our quasi-3D individual-based representation of these cultures we use a discrete, approximate form of the reaction-diffusion system for the morphogen dynamics.

Following this, we present the results of two attempts at modeling the growing 3D limb using different implementations of the Cellular Potts Model, based on energy-minimization of cell-ECM interactions. Unlike the case with the micromass cultures, the geometry of these 3D simulations is necessarily highly idealized relative to the living system. Moreover, in each of these simulations we use slightly different simplifications of the mechanism of Hentschel *et al.* (2004) (Eqs. 1-8), based on different ad hoc separations of the morphogen dynamics from cell movement.

Finally, we have used a novel finite element-based computational strategy to explore the pattern-forming potential of Eqs. 10-11, the morphogen dynamics in the morphostatic limit of system (1)-(8), on irregular spatial domains. Although we have only

accomplished this in 2D thus far, and the active zone of the developing limb (see Fig. 2) constitute 3D domains of changing shape at successive stages of development, this new result and simulation protocol should eventually enable us to return to the 3D framework and implement simulations with more natural shapes and authentic morphogen dynamics.

B. Discrete Stochastic Models

Stochastic discrete models are used in a variety of problems dealing with biological complexity. One motivation for this approach is the enormous range of length scales of typical biological phenomena. Treating cells as simplified interacting agents, one can simulate the interactions of tens of thousands to millions of cells and still have within reach the smaller-scale structures of tissues and organs that would be ignored in continuum (*e.g.*, partial differential equation) approaches. At the same time, discrete stochastic models can be made sophisticated enough to reproduce almost all commonly observed types of cell behavior (Chaturvedi *et al.*, 2003; Chaturvedi *et al.*, 2004; Casal *et al.*, 2005; Alber *et al.*, 2004a,b; Alber, Kiskowski *et al.* 2003, 2004, Sozinova, *et al.*, 2005; 2006).

1. Proof of Principle: Pattern Formation in Mesenchymal Micromass Cultures

We have used a multiscale, stochastic, discrete approach to model chondrogenic pattern formation in vitro in the high-density limb bud mesenchyme micromass culture system (Kiskowski *et al.* 2004; Christley *et al.* 2007). The most recent of these models is multiscale (*i.e.*, cell and molecular dynamics occur on distinct spatial and temporal scales) with cells represented as spatially extended objects that can change their shape (Fig. 4). It has been calibrated using experimental data and simulation results indicate

that cells can form condensation patterns by undergoing small displacements of less than a cell diameter, packing more closely by changing their shapes, while maintaining a relatively uniform cell density across the entire spatial domain.

The simulations have disclosed two distinct dynamical regimes for pattern self-organization involving transient or stationary inductive patterns of morphogens (Fig. 5). The transient regime involves the appearance of morphogen concentrations in a spatial pattern for a brief period of time after which the morphogens are lost from the system by degradation or inactivation. These transient regimes are oscillatory in behavior with the periodic reappearance and degradation of morphogens. The stationary regime involves a spatial pattern of morphogen concentrations that remains stable indefinitely over time. Sensitivity has been studied to changes in key parameters indicating robustness in pattern formation behavior but with variation in the morphological outcomes (Fig. 6). Formation of both spots and stripes of precartilage condensation can be produced by the model under slightly different parameter choices. This corresponds well to experimental results where either morphotype may be generated under similar initial conditions, and it supports the applicability of the core molecular-genetic mechanism we have used to the understanding of both in vitro and in vivo chondrogenic pattern formation.

Tuning of a core molecular-genetic mechanism (*e.g.*, by natural selection or epigenetic factors) can provide both multiple dynamical pathways to the same phenotypic outcome and multiple phenotypes produced from the same dynamical pathway. An important implication is that the limb developmental process does not require a strict progression from one stable dynamical regime to another, but can occur by a succession

of transient dynamical regimes or combination of both regimes to achieve a particular morphological outcome.

2. Simulations of Chondrogenic Patterning in 3D

a. Energetics of Cell Interactions and the Cellular Potts Model. The mesoscopic Cellular Potts Model (CPM), first introduced by Glazier and Graner (1992, 1993), is a cell-level, energy-minimization-based, lattice model that uses an effective energy H coupled to external fields, *e.g.*, the local concentrations of diffusing chemicals, to describe cell-cell interactions, cell adhesion, motion, differentiation, division and apoptosis. The effective energy mixes true energies, such as cell-cell adhesion, with terms that mimic energies, *e.g.*, the response of a cell to a chemotactic or haptotactic gradient. Since the cells' environment is extremely viscous, their motion is entirely dissipative; their motion minimizes their total effective energy consistent with constraints and boundary conditions.

A CPM-based tissue morphogenesis model consists of a list of biological cells, a list of generalized cells, a set of chemical diffusants and a description of the biological and physical behaviors and interactions embodied in the effective energy, along with auxiliary equations to describe secretion, transport and absorption of diffusants and other extracellular materials, state changes within the cell, mitosis and cell death.

In the CPM, *generalized cells* can model non-cellular materials such as ECM and fluid media. Such an approach is much simpler and faster than finite-element modeling, has better spatial fidelity than modeling cells as point particles and can be formally translated into a force-based description of cell behaviors. The CPM discretizes space into a 3D lattice as shown in Fig. 7. Each lattice point contains an integer index that

identifies the cell, ECM element or other object to which it belongs. Separate lattices contain concentrations of diffusants, which evolve under partial differential equations (PDEs), while sets of state maps and ordinary differential equations (ODEs). The effective energy mixes true energies, like cell-cell adhesion, and terms that mimic energies, *e.g.*, the response of a cell to a chemotactic gradient.

The configuration evolves through attempts to copy an index from a site into a neighboring site with a different index. This index copy changes the effective energy and we accept the change with a probability that depends on the change of energy ΔE due to the copy according to an acceptance function

$$\Phi(\Delta E) = \begin{cases} 1, & \Delta E \le 0 \\ e^{-\frac{\Delta E}{T}}, & \Delta E > 0 \end{cases} \qquad (13)$$

where T represents an effective boundary fluctuation amplitude of model cells in units of energy. Thus the pattern evolves (and cells move) to minimize the total effective energy. This algorithm implements Metropolis dynamics with Monte-Carlo Boltzmann acceptance (see Newman and Barkema, 1999).

b. 3D CPM-Based Limb Simulations. Chaturvedi *et al.* (2005) and Cickovski *et al.* (2005; 2007) have presented a unified, object-oriented, three-dimensional biomodelling environment. This framework allows the integration of multiple submodels at scales from subcellular to those of tissues and organs. The implementations in each case combined a modified CPM with a continuum reaction–diffusion model and a state automaton with well-defined conditions for cell differentiation transitions to model genetic regulation. This environment allows one to rapidly and compactly create computational models of a class of complex-developmental phenomena. Cickovski *et al.*

(2005) describes in detail a computational package, CompuCell3D[1], based on the hybrid modeling approach.

CPM-based simulations of vertebrate limb development in this multiscale, multi-model simulation environment are presented in both Chaturvedi *et al.* (2005) and Cickovski *et al.* (2005). The biological basis of each set of simulations was that described above: the "bare-bones" mechanism of Hentschel *et al.* (2004), projected onto the geometry of Fig. 3, but with the third, dorsoventral, dimension made explicit. Both studies separated the morphogen dynamics from cell rearrangement (intrinsically connected to each other in system (1)-(8)) using different ad hoc simplifications to obtain a two-equation PDE system for activator-inhibitor interactions.

Beyond this, each of the analyses used a different set of additional simplifications to make the 3D simulations tractable. Chaturvedi *et al.* (2005), for example, used the full range of cell types, R_1, R_2, $R_2^{'}$ and R_3 in its cell-state transition map, whereas Cickovski *et al.* (2005) modeled only "noncondensing" and "condensing" cells. Chaturvedi *et al.* (2005) induced transitions between patterns in the different proximodistal domains of the developing limb by changing the values of the morphogen diffusion coefficients, which is formally equivalent to the biologically-justified alteration of the aspect ratio of the active zone (Newman and Frisch, 1979; Hentschel *et al.*, 2004). Successive stationary patterns were then computed. In Cickovski *et al.* (2005), the width of the active zone changed in an "automatic," or self-organizing, fashion by incorporating into the model the movement of proliferating cells away from the high point of FGF at the AER. Additional details can be found in the respective papers.

[1] [1] https://simtk.org/home/compucell3d

Examples of 3D simulations of TGF-β, fibronectin and condensation patterns from these two studies are shown in (Fig. 8). The similarities in the results, and the rough fidelity to actual development (*e.g.*, proximodistal emergence of increasing numbers of elements) despite the varying simplifications used, are encouraging with regard to the validity of the common underlying assumptions.

C. Continuum models

In continuum models some entities that are inherently discrete and exist in finite numbers are modeled instead by a continuous variable. This can be justified if the entities are present in large numbers, and the scale on which they are observed is much larger than the scale of entities themselves. Continuum models use families of differential or integro-differential equations to describe "fields" of interaction. Discrete models describe individual (microscopic) behaviors. They are often applied to micro-scale events where a small number of elements can have a large (and stochastic) impact on a system. When we model organogenesis, such as vertebrate limb development, morphogen production and diffusion are on the molecular level, which has a much smaller scale than the cell level. Since our observations are on the cell and tissue levels, continuum models will work well for limb bud shaping and morphogen evolution, components of our multiscale model. We use reaction-diffusion PDEs to model diffusing morphogen molecules and their biochemical reactions. Efficient numerical methods for reaction-diffusion equations can be used to simulate the reaction-diffusion models. In contrast, modeling the motion of individual morphogen molecules by discrete methods would be computationally too costly, due to the huge number of morphogen molecules in our multiscale model.

1. Morphogen Dynamics on an Irregular Domain

Patterns in reaction-diffusion systems depend sensitively on domain size and shape (Lyons and Harrison, 1992; Crampin *et al.*, 2002; Zykov and Engel, 2004). Since the natural shape of a limb bud, and its subdomains such as the active zone (see Fig. 2) have non-standard geometries, we developed a mathematical formalism based on the Galerkin method (Johnson, 1987), to handle the complicated geometries and solve morphostatic reaction-diffusion system (9-10) numerically. The Galerkin method is a means for converting an ordinary or partial differential equation system into to a problem represented by a system of algebraic equations in a more restricted space than that of the original system. Since it is a "variational" method, it employs "test functions" to approximate the system's behavior on the restricted space.

a. The Discontinuous Galerkin Finite Element Method. Our formalism, the *Discontinuous Galerkin finite element* (DGFE) method, is termed "discontinuous" due to the usage of completely discontinuous piecewise polynomial space for the numerical solution and the test functions. Major advances in the use of this approach were presented in a series of papers by Cockburn *et al.* (1989; 1990; 1991; 1998).

DG methods have several advantages that make them attractive for biological applications. These include their ability to easily handle complicated geometry and boundary conditions (an advantage shared by all finite element methods), their flexibility in using polynomials with different orders on neighboring elements to approximate the solution of the differential equation, and their permitting the use of very irregular computational meshes. These properties of DG methods make it much easier to incorporate adaptivity technique (an important technique to save computational cost) than

other numerical methods. DG methods are also compact and hence efficient in parallel implementation. They also can be easily coordinated with finite volume techniques for applying to problems with discontinuous or sharp gradient solutions.

Recently, Cheng and Shu (2006) developed a new DG method for solving time dependent PDEs with higher order spatial derivatives. The scheme is formulated by repeated integration by parts of the original equation and careful treatment of the discontinuity of the numerical solutions on the interface of the neighboring elements, which is important for the stability of the DG method. It is easier to formulate and implement, needs less storage and CPU cost than the usual DG method for PDEs with higher order spatial derivatives.

We adopted discontinuous Galerkin finite element (DGFE) numerical approaches of Cheng and Shu (2006) and implemented it on both 2D rectangular and triangular meshes to solve the reaction-diffusion system (10)-(11). The spatial discretization by the DG method will transform the reaction-diffusion PDEs to a system of ODE. Due to the stiffness nature of the reaction-diffusion system, it will be computationally expensive if regular ODE integrators are used. We adopted Strang's operator splitting technique (Strang, 1968) and the Crank-Nicholson discretization for stiff systems (Chou *et al.*, 2007) to achieve more efficient simulations than afforded by regular ODE integrators.

Patterns in reaction-diffusion systems are sensitive to the domain size and geometrical shape. The shape of the developing limb bud undergoes continuous changes. The DG finite element approach can handle the irregular shapes easily by using triangular meshes to fit the domain. Both spot-like and stripe-like patterns are observed in simulations of the steady state of the reaction-diffusion system (10)-(11), derived in the

morphostatic limit. To simulate the pattern of realistic shapes of morphogenetically active zones in the limb bud, we randomly perturbed the rectangular boundary of the active zone, and used triangular mesh to fit the irregular boundary. In Fig. 9, the triangular meshes were presented to show the fit of computational mesh to the irregular boundary. The vertical length of the domain is roughly 0.65, and the horizontal length is 0.15. A flood contour plot of the steady-state of the concentration of the activator c_a is shown. Different colors in the domain represent different values of c_a. We achieved stripe-like patterns as shown in Fig. 9. To examine the pattern dependence on the ratio of horizontal length and vertical length of the active zone, we fixed the vertical length to be 1, but changed the horizontal length successively. The steady state patterns are shown in Fig. 10, and we can observe the changing of stripe-like patterns to spot-like patterns when the horizontal length is increased. The parameters in the system (10)-(11) for Fig. 9 and Fig. 10 are taken to be

$$D_a = 1,\ D_i = 50.3,\ J_a^1\alpha = 0.05\gamma,\ J_{a\max} = 6.0\gamma,\ J_{i\max} = 8.0\gamma,\ k_a = \gamma,$$
$$\beta_1 = 0.693473,\ \beta_2 = 2.66294,\ R_{eq} = 2.0,\ n = q = 2,\ \gamma = 8900,\ s = 4.0,\ \delta = 4.8.$$

V. Discussion and Future Directions

While the reactor-diffusion mechanism for vertebrate limb development has yet to be confirmed in an unequivocal fashion, it is the only available model that accounts for the spatiotemporal increase skeletal elements seen in all amniote species (reptiles, birds, mammals) in a natural fashion. We have found that under slightly different assumptions from our "bare-bones" mechanism (Hentschel *et al.*, 2004; Eqs. 1-8, above), which take account of the differences in tissue sources of key FGFs in urodele amphibians (Han *et*

al., 2001), our model can even account for the deviations from the proximodistal order of skeletogenesis in those species (Franssen *et al.*, 2005; Glimm and Newman, in preparation).

The reactor-diffusion model for limb development has clear affinities to the increasingly well-established "clock and wavefront" model for somitogenesis (Cooke and Zeeman, 1976; Pourquié, 2003; Baker *et al.*, Schnell *et al.*, this volume). Specifically, in both models mesenchymal cells become susceptible to a periodic patterning signal by escaping the suppressive activity of a gradient of FGF. In somitogenesis the periodic signal, which sweeps along the length of the presomitic mesoderm, is a Notch and Wnt-based molecular oscillator with both temporal and spatial aspects. In the limb, the molecular mechanism presumed to generate the condensation-inducing chemical standing waves is more elusive, not least because the nature of the lateral inhibitor remains unknown (but see Moftah *et al.*, 2002 and Fujimaki *et al.*, 2006). Measurement of morphogen diffusion rates in living tissues is notoriously difficult (Lander, 2007) and the reactor-diffusion mechanism may thus be difficult to subject to definitive tests for some time. A promising route to a partial test of this model is suggested by experimental evidence for temporal periodicities in the response of micromass cultures to perturbation by TGF-β (Leonard *et al.*, 1991). As noted above, discrete stochastic simulations of this culture system disclose a temporally periodic dynamical regime (Christley *et al.*, 2007; Fig. 5A) and analysis of the PDE system (1)-(8) under conditions in which diffusion is suppressed shows it to have strong oscillatory modes (Hentschel and Newman, in preparation). Recent observations that Notch-related signaling components undergo

temporal oscillations in limb mesenchyme (Bhat and Newman, unpublished) strengthen the presumption of an underlying reactor-diffusion patterning mechanism.

While the morphostatic limit for the system (1)-(8) was introduced to make analysis of morphogen patterns more tractable, it may also represent a reality of development for most or some tetrapod embryos. The establishment of the limb skeletal pattern in chickens occurs over 4 days, while the same process in humans occurs over 4 weeks. Since the spatial scales of limb development in the two species are similar, one or more dynamical processes – morphogen evolution, cell differentiation, cell mobility – must differ substantially. This indicates that the parameters determining rates of development, including, but not confined to those in the "bare-bones" formulation, have been subject to natural selection. Transformation of an inherently morphodynamic system into a morphostatic one by, for example, slowing the rate of cell movement, is a plausible evolutionary scenario for the limb and for other developmental systems, making them more resistant to radical changes in morphology when key genes are mutated (Salazar-Ciudad *et al.*, 2003; Salazar-Ciudad, 2006).

Simulating morphogen dynamics in irregularly shaped domains, as indicated above, is a necessary step to generating an authentic limb model. But rather than the domain shapes being chosen arbitrarily, ultimately they must arise from the material properties of the limb bud. Two major modifications need to be made to the 3D modeling strategy described in section IVB2 before it has a real possibility of capturing the essence of the developing limb. First, the growing limb bud needs to be modeled as a naturally shaped object with a curvilinear profile in all three dimensions. Thus far our 2D and 3D simulations have all used rectangular shapes (Hentschel *et al.*, 2004) and parallelepipeds

(Chaturvedi *et al.*, 2005; Cickovski *et al.*, 2005). Modeling of shape change in developing systems has attracted much attention in recent years, with applications ranging from growth of tumors (Araujo *et al.*, 2004) and hydroid polyps (Beloussov *et al.*, 2006) to the developing human brain (Czanner *et al.*, 2001). The limb mesenchyme is a viscous material ensheathed by the ectoderm, a viscoelastic sheet. Murea and Hentschel (2007) have presented a finite element strategy for modeling limb bud outgrowth as a problem in creeping viscous flow under nonuniform surface tension in a (2D) system with a free-moving boundary. This continuously reshaped form, particularly in a 3D extension, would constitute a realistic supporting medium and set of boundaries for both the morphogen dynamics (*e.g.*, Eqs. 10-11), and the model cells of the CPM or its equivalent, in a hybrid model that includes morphogenesis as well as skeletal pattern formation.

Finally, the limb and its skeleton are not symmetrical. Although little is known about how they do so, the various gradients in the limb bud, *e.g.*, Sonic hedgehog emanating from the posterior Zone of Polarizing Activity (ZPA), various Hox proteins distributed along the proximodistal and anteroposterior axes, and Wnt7A distributed along the dorsoventral axis, influence the size and shapes of the various skeletal elements and endow the limb with polarity along these axes. Computational models such as those described here afford a way of testing hypotheses for the action of these modulating factors. By default, under symmetric conditions, simulations with the models described above lead to model skeletons with no distinction among the different elements, other than they increase in number along the proximodistal axis as development proceeds (Fig. 8). By making the reasonable assumption that the graded modulators act on the

efficiency and strength of components of the core mechanism (*e.g.*, how much fibronectin is produced per unit of TGF-β; how efficient the inhibitor is in suppressing TGF-β) it should be possible to introduce such uniformities into the various models and observe the effects on the simulated limb morphologies. As these models becomes richer in genetic interactions and potentially more realistic, they can help explain the outcomes of experimental manipulations and effects of medically relevant mutations in the vertebrate limb, and suggest hypotheses for its evolutionary origination and diversification.

References

Alber, M.S., Kiskowski, M.A., *et al.* (2003). On cellular automaton approaches to modeling biological cells, in J. Rosenthal and D.S. Gilliam (Eds.), *Mathematical Systems Theory in Biology, Communication, and Finance*, IMA Volume 134, Springer-Verlag, New York, 1-39, 2003.

Alber, M., Kiskowski, M.A. *et al.* (2004). Biological lattice gas models, in *Dynamics and Bifurcation of Patterns in Dissipative Systems*, G. Dangelmayr and I. Oprea (eds.), World Scientific Series on Nonlinear Science, Vol. 12, World Scientific, Singapore, 274-291.

Alber, M., Hentschel, H.G.E. *et al.* (2005). Existence of solutions to a new model of biological pattern formation. *J. Math. Anal. Appl.* **308,** 175-194.

Alber, M., Glimm, T. *et al.* (2005). Stability of n-dimensional patterns in a generalized Turing system: implications for biological pattern formation, *Nonlinearity* **18,** 125-138.

Alber, M., Chen, N. *et al.* (2006). Multiscale dynamics of biological cells with chemotactic interactions: From a discrete stochastic model to a continuous description, *Phys. Rev. E*. 73, 051901.

Alber, M., Glimm, T. *et al.* The morphostatic limit for a model of skeletal pattern formation in the vertebrate limb. (submitted; in revision).

Araujo R., and D. McElwain (2004). A history of the study of solid tumour growth: the contribution of mathematical modeling, *Bull. Math. Biol.* **66,** 1039-1091.

Borkhvardt VG. 2000. The growth and form development of the limb buds in vertebrate animals. *Ontogenez* **31,** 192-200.

Beloussov, L.V. and V.I. Grabovsky (2006). Morphomechanics: goals, basic experiments and models, *Int. J. Dev. Biol.* 50, 81-92.

Casal, A., Sumen, C. *et al.* (2004). A cellular automata model of early T cell recognition, Lecture Notes in Computer Science, Springer-Verlag, Vol. 3305, Springer-Verlag, New York, 553-560.

Casal, A., Sumen, C. *et al.* (2005). Agent-based modeling of the context dependency in T cell recognition, *J. Theor. Biol.* **236,** 376-391.

Chaturvedi, R., J.A. Izaguirre *et al.* (2003). Multi-model simulations of chicken limb morphogenesis, Lecture Notes in Computer Science, Volume 2659, Springer-Verlag, New York, 39-49.

Chaturvedi, R., Huang, C. *et al.* (2004). A hybrid discrete-continuum model for 3-D skeletogenesis of vertebrate limb, Lecture Notes in Computer Science, Vol. 3305, Springer-Verlag, New York, pp. 543-552.

Chaturvedi, R., Huang, C. *et al.* (2005b). On Multiscale Approaches to 3-Dimensional Modeling of Morphogenesis, *J. R. Soc. Interface* **2,** 237-253.

Chen, N, Glazier, J.A., and Alber, M.S. (2006a). A parallel implementation of the Cellular Potts Model for simulation of cell-based morphogenesis, S. El Yacoubi, B. Chopard, and S. Bandini (Eds.): ACRI 2006, LNCS 4173, Springer-Verlag Berlin Heidelberg, pp. 58-67.

Chen, N., Glazier, J.A. *et al.* (2006b). A parallel implementation of the Cellular Potts Model for simulation of morphogenesis (submitted).

Cheng, Y., and Shu, C.-W. A discontinuous Galerkin finite element method for time dependent partial differential equations with higher order derivatives**,** *Math. Computat.*, to appear.

Chou, C.-S., Zhang, Y.-T. *et al.* (2007). Numerical methods for stiff reaction-diffusion systems*, Discrete Contin. Dynam. Syst., Ser. B,* **7,** 515-525.

Christley, S., Alber, M.S., and Newman, S.A. (2007). Patterns of mesenchymal condensation in a multiscale, discrete stochastic model. *PLoS Computat. Biol.* **3,** e76.

Cickovski, T., C. Huang, R. Chaturvedi, T. Glimm, H.G.E. Hentschel, M. Alber, J. A. Glazier, S. A. Newman, J. A. Izaguirre (2005). A Framework for Three-Dimensional Simulation of Morphogenesis, *IEEE/ACM Trans. Computat. Biol. Bioinform.* **2,** 273-288.

Cickovski, T., A. Kedar, M Swat, R.M.H. Merks, T. Glimm, H.G.E. Hentschel, M.S. Alber, J.A. Glazier, S.A. Newman, J.A. Izaguirre (2007). From genes to organisms via the cell: a problem solving environment for multicellular development. *Comput. Sci. Engineer.*, in press.

Cockburn, B. (1999). Discontinuous Galerkin methods for convection-dominated problems, in High-Order Methods for Computational Physics, T.J. Barth and H. Deconinck, editors, Lecture Notes in Computational Science and Engineering, volume 9, Springer, pp 69-224.

Cockburn, B., Lin S.-Y., and Shu, C.-W. (1989). TVB Runge-Kutta local projection discontinuous Galerkin finite element method for conservation laws III: one dimensional systems, *J. Computat. Physics* **84,** 90-113.

Cockburn, B., Hou, S., and Shu, C.-W. (1990). The Runge-Kutta local projection discontinuous Galerkin finite element method for conservation laws IV: the multidimensional case, *Math. Computat.* **54,** 545-581.

Cockburn, B. and Shu, C.-W. (1989). TVB Runge-Kutta local projection discontinuous Galerkin finite element method for conservation laws II: general framework, *Math. Computat.*, **52,** 411-435.

Cockburn, B., and Shu, C.-W. (1991). The Runge-Kutta local projection P1-discontinuous Galerkin finite element method for scalar conservation laws, *Math. Modelling Numer. Anal.* **25**, 337-361.

Cockburn, B., and Shu, C.-W. (1998). The local discontinuous Galerkin finite element method for convection-diffusion system. *SIAM J. Numer. Anal.* **35,** 2440-2463.

Cockburn, B., and Shu, C.-W. (1998). The Runge-Kutta discontinuous Galerkin method for conservation laws V: multidimensional systems, *J. Computat. Physics* **141,** 199-224.

Cockburn, B., and Shu, C.-W. (1998). The local discontinuous Galerkin method for time-dependent convection-diffusion systems, *SIAM J. Numer. Anal.* **35,** 2440-2463.

Cooke, J., and Summerbell, D. (1981). Control of growth related to pattern specification in chick wing-bud mesenchyme. *J. Embryol. Exp. Morphol.* **65 Suppl,** 169-185.

Cooke, J., and Zeeman, E. C. (1976). A clock and waterfront model for the control of repeated structures during animal morphogenesis, J. Theor. Biol. **58,** 455-476.

Crampin, E.J., Hackborn, W.W. and M.K. Maini (2002). Pattern formation in reaction-diffusion models with nonuniform domain growth. *Bull Math Biol.* **64,** 747-69.

Czanner, S, R. Durikovic, and H. Inoue (2001). Growth simulation of human embryo brain, *17th Spring Conference on Computer Graphics (SCCG '01)*, p. 0139.

Dillon, R., and H. G. Othmer (1999). A mathematical model for outgrowth and spatial patterning of the vertebrate limb bud, *J. Theor. Biol.* **197,** 295-330.

Dorfman, R., and Shilo, B.Z. (2001). Biphasic activation of the BMP pathway patterns the *Drosophila* embryonic dorsal region. *Development* **128,** 965-975.

Downie, S.A., and Newman, S.A. (1994). Morphogenetic differences between fore and hind limb precartilage mesenchyme: relation to mechanisms of skeletal pattern formation. *Develop. Biol.* **162,**195-208.

Dubrulle, J., McGrew, M. J., and Pourquié, O. (2001). FGF signaling controls somite boundary position and regulates segmentation clock control of spatiotemporal Hox gene activation. *Cell* **106,** 219-32.

Dudley, A. T., Ros, M. A., and Tabin, C. J. (2002). A re-examination of proximodistal patterning during vertebrate limb development. *Nature* **418,** 539-44.

Enderling, H, A. Anderson, M. *et al.*, Visualisation of the numerical solution of partial differential equation systems in three space dimensions and its importance for mathematical models in biology, *Math. Biosci. Engineer.*, to appear.

Filion, R.J., and Popel, A.S. (2004). A reaction-diffusion model of basic fibroblast growth factor interactions with cell surface receptors. *Ann. Biomed. Eng.* **32,** 645-663.

Forgacs, G., and Newman, S.A.. (2005). Biological physics of the developing embryo. Cambridge: Cambridge Univ. Press.

Franssen, RA, Marks, S. *et al.* (2005). Limb chondrogenesis of the seepage salamander, *Desmognathus aeneus* (Amphibia: Plethodontidae). *J. Morphol*. **265,** 87-101.

Fujimaki, R., Toyama, Y. *et al.* (2006). Involvement of Notch signaling in initiation of prechondrogenic condensation and nodule formation in limb bud micromass cultures. *J. Bone Miner. Metab.* **24,** 191-198.

Glazier, J.A., and Graner, F. (1993). A simulation of the differential adhesion driven rearrangement of biological cells. *Phys. Rev. E Stat. Nonlin. Soft Matter Phys.* **47,** 2128-2154.

Graner, F., and Glazier, J.A. (1992). Simulation of biological cell sorting using a two-dimensional extended Potts model. *Physical Review Letters* **69,** 2013-2016.

Hall, B.K., and Miyake, T. (1995). Divide, accumulate, differentiate: cell condensation in

skeletal development revisited. *Int. J. Dev. Biol.* **39,** 881-893.

Hall, B. K., and Miyake, T. (2000). All for one and one for all: condensations and the initiation of skeletal development. *Bioessays* **22,** 138-147.

Han, M. J., An, J. Y., and Kim, W. S. (2001). Expression patterns of FGF-8 during development and limb regeneration of the axolotl. *Dev. Dyn.* **220,** 40-8.

Hentschel, H.G.E., Glimm, T. *et al.* (2004). *Proc. Roy. Soc. Lond.* B **271,** 1713-1722.

Kiskowski, M.A., Jiang, Y., and Alber, M.S. (2004). Role of streams in *Myxobacteria* aggregate formation, *Phys. Biol.* **1,** 173-183.

Kiskowski, M., Alber, M. *et al.* (2004). Interplay between activator-inhibitor coupling and cell-matrix adhesion in a cellular automaton model for chondrogenic patterning. *Dev. Biol.* **271**, 372-387.

Kosher, R.A., Savage, M.P., and Chan, S.C. (1979). In vitro studies on the morphogenesis and differentiation of the mesoderm subjacent to the apical ectodermal ridge of the embryonic chick limb-bud. *J. Embryol. Exp. Morphol.* **50,** 75-97.

Izaguirre, J.A., Chaturvedi, R. *et al.* (2004). CompuCell, a multi-model framework for simulation of morphogenesis, *Bioinformatics* **20,** 1129-1137.

Jiang, T. X., Widelitz, R. B. *et al.* (2004). Integument pattern formation involves genetic and epigenetic controls: feather arrays simulated by digital hormone models. *Int. J. Dev. Biol.* **48,** 117-35.

Johnson, C. (1987). Numerical solution of partial differential equations by the finite element method, Cambridge University Press, Cambridge, New York.

Lander, A.D. (2007). Morpheus unbound: reimagining the morphogen gradient. *Cell* **128,** 245-256.

Lander, A.D., Nie, Q., and Wan, F.Y. (2002). Do morphogen gradients arise by diffusion? *Dev. Cell* 2:785-796.

Leonard, C.M., Fuld, H.M. *et al.* (1991). Role of transforming growth factor-β in chondrogenic pattern formation in the embryonic limb: stimulation of mesenchymal condensation and fibronectin gene expression by exogenous TGF-β and evidence for endogenous TGF-β-like activity. *Dev. Biol.* **145,** 99-109.

Litingtung, Y., Dahn, R. D. *et al.* (2002). Shh and Gli3 are dispensable for limb skeleton

formation but regulate digit number and identity. *Nature* **418,** 979-83.

Lyons, M.J., Harrison, L.G. (1992). Stripe selection: an intrinsic property of some pattern-forming models with nonlinear dynamics. *Dev. Dyn.* **195,** 201-215.

Maini, P. K., Baker, R. E., and Chuong, C. M. (2006). Developmental biology. The Turing model comes of molecular age. *Science* **314,** 1397-8.

Mariani, F.V., and Martin, G.R. (2003). Deciphering skeletal patterning: clues from the limb. *Nature* **423,** 319-325.

Martin, G.R. (1998). The roles of FGFs in the early development of vertebrate limbs. *Genes Dev*. **12,** 1571-1586.

Merks, R.M.H., Brodsky, S.V. *et al.* (2006). Cell elongation is key to in silico replication of in vitro vasculogenesis and subsequent remodeling. *Dev. Biol.* **289,** 44-54.

Miura, T., and Maini, P.K. (2004). Speed of pattern appearance in reaction-diffusion models: implications in the pattern formation of limb bud mesenchyme cells. *Bull. Math Biol.* **66,** 627-49.

Miura ,T., and Shiota, K. (2000). Extracellular matrix environment influences chondrogenic pattern formation in limb bud micromass culture: experimental verification of theoretical models. *Anat Rec.* **258,** 100-107.

Miura, T., and Shiota, K. (2000). TGFβ2 acts as an "activator" molecule in reaction-diffusion model and is involved in cell sorting phenomenon in mouse limb micromass culture. *Dev. Dyn.* **217,** 241-249.

Miura, T., Shiota, K. *et al.* (2006). Mixed-mode pattern in Doublefoot mutant mouse limb—Turing reaction-diffusion model on a growing domain during limb development. *J. Theor. Biol.* **240,** 562-573.

Moftah, M.Z., Downie, S.A. *et al.* (2002). Ectodermal FGFs induce perinodular inhibition of limb chondrogenesis in vitro and in vivo via FGF receptor 2. *Dev. Biol.* **249.** 270-282.

Mizutani, C.M, Nie, Q. *et al.* (2005). Formation of the BMP activity gradient in the *Drosophila* embryo. *Dev. Cell.* **8,** 915-924.

Murea, C. M., and Hentschel, H. G. E. (2007). A finite element method for growth in biological development. *Math. Biosci. Eng.* **4,** 339-353.

Newman, S. A. (1988). Lineage and pattern in the developing vertebrate limb. *Trends Genet.* **4,** 329-332.

Newman, S.A. (1996). Sticky fingers: Hox genes and cell adhesion in vertebrate limb development. *BioEssays* **18,** 171-174.

Newman, S.A., and Frisch, H. (1979). Dynamics of skeletal pattern formation in developing chick limb, *Science* **205,** 662-668.

Newman, S.A., Frisch, H.L. *et al.* (1981). Limb development: aspects of differentiation, pattern formation and morphogenesis. In: Connolly TG, Brinkley LL, Carlson BM, editors. Morphogenesis and Pattern Formation. Raven Press, New York. pp 163-178.

Newman, S.A., and Muller, G.B. (2005). Origination and innovation in the vertebrate limb skeleton: an epigenetic perspective. *J. Exp. Zoolog. B Mol. Dev. Evol.* **304,** 593-609.

Niswander L, Tickle C, Vogel A, Booth I, Martin GR. 1993. FGF-4 replaces the apical ectodermal ridge and directs outgrowth and patterning of the limb. Cell 75:579-587.

Nie, Q, Y.T. Zhang and R. Zhao (2006). Efficient semi-implicit schemes for stiff systems, *J. Computat. Phys.*, **214,** 521-537.

Ornitz, D.M., and Marie, P.J. (2002). FGF signaling pathways in endochondral and intramembranous bone development and human genetic disease. *Genes Dev.* **16,** 1446-1465.

Peters, K.G., Werner, S. *et al.* (1992). Two FGF receptor genes are differentially expressed in epithelial and mesenchymal tissues during limb formation and organogenesis in the mouse. *Development* **114,** 233-243.

Pourquié, O. (2003). The segmentation clock: converting embryonic time into spatial pattern. *Science* **301,** 328-30.

Ros, M. A., Lyons, G. E. *et al.* (1994). Recombinant limbs as a model to study homeobox gene regulation during limb development. *Dev. Biol.* **166,** 59-72.

Salazar-Ciudad, I. (2006). On the origins of morphological disparity and its diverse developmental bases. *BioEssays* **28,** 1112-22.

Salazar-Ciudad, I., and Jernvall, J. (2002). A gene network model accounting for development and evolution of mammalian teeth. *Proc Natl Acad Sci U S A* **99,** 8116-20.

Salazar-Ciudad. I., Jernvall, J., and Newman, S.A. (2003). Mechanisms of pattern formation in development and evolution. *Development* **130,** 2027-2037.

Saunders, J.W., Jr. (1948). The proximo-distal sequence of origin of the parts of the chick wing and the role of the ectoderm. *J. Exp. Zool.* **108,** 363-402.

Sick, S., Reinker, S. *et al.* (2006). WNT and DKK determine hair follicle spacing through a reaction-diffusion mechanism. *Science* **314,** 1447-50.

Sozinova, O., Jiang, Y. *et al.* (2006a). A three-dimensional model of Myxobacterial aggregation by contact-mediated interactions, *Proc. Natl. Acad. Sci. USA* **102,** 11308-11312.

Sozinova, O., Jiang, Y. *et al.* (2006b), A three-dimensional model of fruiting body formation, *Proc. Natl. Acad. Sci. USA* **103,** 17255-17259.

Strang, G. (1968). On the construction and comparison of difference schemes, *SIAM J. Numer. Anal.* **5,** 506-517.

Szebenyi, G., Savage, M.P., *et al.* (1995). Changes in the expression of fibroblast growth factor receptors mark distinct stages of chondrogenesis in vitro and during chick limb skeletal patterning. *Dev. Dyn.* **204,** 446-456.

Tickle, C. (2003). Patterning systems-from one end of the limb to the other. *Dev. Cell* **4,** 449-458.

Turing, A. (1952). The chemical basis of morphogenesis. *Phil. Trans. Roy. Soc. Lond.* B **237,** 37-72.

Van Obberghen-Schilling, E,, Roche, N.S. *et al.* (1988). Transforming growth factor beta-1 positively regulates its own expression in normal and transformed cells. *J. Biol. Chem.* **263,** 7741-7746.

Williams PH, Hagemann A, Gonzalez-Gaitan M, Smith JC. 2004. Visualizing long-range movement of the morphogen Xnr2 in the Xenopus embryo. *Curr. Biol.* **14,** 1916-1923.

Xu, Y and C.-W. Shu (2005). Local discontinuous Galerkin methods for two classes of two-dimensional nonlinear wave equations, *Physica D* **208,** 21-58.

Yamaguchi, M., Yoshimoto, E., and Kondo, S. (2007). Pattern regulation in the stripe of zebrafish suggests an underlying dynamic and autonomous mechanism. *Proc Natl Acad Sci U S A* **104,** 4790-3.

Yan, J and Shu, C.-W. (2002). A local discontinuous Galerkin method for KdV type equations, *SIAM J. Numer. Anal.* **40,** 769-791.

Yokouchi, Y., Nakazato, S. *et al.* (1995). Misexpression of *Hoxa-13* induces cartilage homeotic transformation and changes cell adhesiveness in chick limb buds. *Genes Dev.* **9,** 2509-2522.

Zhang Y.T., Lander, A., and Nie, Q. Computational analysis of BMP gradients in dorsal-ventral patterning of the zebrafish embryo, in press.

Zheng, Y.T., Wise, X.S.M., and Cristini, V. (2005). Nonlinear simulation of tumor necrosis, neo-vascularization and tissue invasion via an adaptive finite-element/level-set method, *Bull. Math. Biol.* **67,** 211-259.

Zykov, V., and Engel, H. (2004). Dynamics of spiral waves under global feedback in excitable domains of different shapes. *Phys. Rev. E Stat. Nonlin. Soft Matter Phys.* 70:016201.

Figure Legends

Fig. 1. Progress of limb skeletal development in chicken forelimb (wing) between 3 and 7 days of embryogenesis. Gray represents precartilage condensation and black represents definitive cartilage. The limb bud, is paddle-shaped, being narrower in the dorsoventral dimension than in anteroposterior or the shoulder-to-finger tips direction in which it mainly grows.

Fig. 2. The interactions of the core mechanism are superimposed on a 2-dimensional schematic limb bud organized into zones defined by experimentally-determined expression patterns of FGF receptors 1, 2 and 3. In the apical zone cell rearrangement is suppressed by the FGFs emanating from the AER. The active zone, a detailed view of which is shown below) is the site of spatiotemporal regulation of mesenchymal cell condensation (*i.e.*, pattern formation). When cells leave the proximal end of the active zone and enter the frozen zone they differentiate into cartilage and their spatiotemporal pattern becomes fixed. The length of the dorsoventral axis is collapsed to zero in this simplified model. PD: proximodistal; AP anteroposterior. In lower panel, curved arrows: positively autoregulatory activator; lines ending in circles: lateral inhibitor. (See Hentschel *et al.*, 2004).

Fig. 3. Core set of cell-gene product interactions leading to limb precartilage mesenchymal condensation. The molecular identity of the lateral inhibitor of condensation is unknown, but depends on interaction of ectodermal FGFs with mesenchymal FGF receptor 2 (Moftah *et al.*, 2002) as well as the Notch signaling pathway (Fujimaki *et al.*, 2006). This inhibitor may act at the level of TGF-β synthesis or activity (solid inhibitory vector), fibronectin synthesis (dashed inhibitory vector), or at some earlier stage. For the purposes of our computational model, we assume it acts on the activator (*i.e.*, TGF-β).

Fig. 4. Multipixel spatial representation of limb mesenchymal cells. (A) Three cells on the spatial grid each occupying seven pixels. (B) Cell changes shape. The region of the cell that contains the nucleus, indicated by the four gray pixels, is structurally maintained;

two border pixels move to new locations, and one border pixel (top right) displaces a nucleus pixel which gets shifted to the right. (C) Cell rounding-up on fibronectin. The surface area in the presence of suprathreshold amounts of fibronectin is reduced with two border pixels moving into a quasi–third dimension above the cell.

Fig. 5. Dynamics of Oscillatory and Stationary Regimes

(A) Oscillatory regime produces transient patterns that repeat over time but are spatially stochastic. (B) Stationary regime produces stable patterns with minor stochastic fluctuations around an equilibrium concentration. Graphs show the maximum concentration value for a single pixel across the entire molecular grid for activator (black) and inhibitor (blue) morphogens.

Fig. 6. Variation in some of the key parameters induces morphological changes in the resultant spatial patterns from distinct spots to connected spots to stripe-like patterns. Average peak interval versus average island size for variations in the some of the key parameters are shown: +5% (diamond) and -5% (filled diamond) for activator self-regulation (k_1), +5% (triangle) and -5% (filled triangle) for activator regulation of inhibitor (k_3), +5% (down triangle) and -5% (filled down triangle) for inhibitor regulation of activator (k_2), +5% (plus) for inhibitor decay (k_4). The colored points are a gradient of variations: 1% (red), 2% (orange), 3% (green), 4% (blue), 5% (violet). Also shown are the five simulations (square) using the standard parameter values in Table 2 and the mean for the twelve experiments (circle). All simulations were run for 3000 iterations with periodic boundary conditions.

Fig. 7. A typical 2D CPM configuration. The numerals indicate indices at lattice sites. The colors indicate cell type. A cell is collection of connected lattice points with same index. The number of lattice points in a cell is its volume and its number of links with other indices is its surface area. We represent ECM as a generalized cell with index 1.

Fig. 8. (a) CompuCell3D simulation of distribution of TGF-β (activator) over progressive developmental stages (time increasing from bottom to top); (b) CompuCell3D simulation of cell condensation into humerus (lower), ulna and radius

(middle), and digits (top) after 1040 Monte Carlo steps. Visualization was produced using volume rendering; (c) CompuCell3D simulation successive stages (top to bottom) of proximodistal development of limb skeleton. Panels (a) and (b) from Chaturvedi *et al.* (2005); panel (e) from Forgacs and Newman (2005), based on Cickovski *et al.* (2005), courtesy of Trevor Cickovski.

Fig. 9. Simulations on the active zone with an irregular shape. Contour plots of the steady state of the concentration of the activator. A triangular mesh is used to fit the irregular boundary of the domain. The vertical length of the domain is roughly 0.65, and the horizontal length is 0.15. $\delta = 4.8$

Fig. 10. Simulations on active zones with changing sizes in the horizontal direction, and the vertical size fixed at 1. Contour plots of the steady states of concentrations of the activator for different domain size. Triangular meshes are used. $\delta = 4.8$.

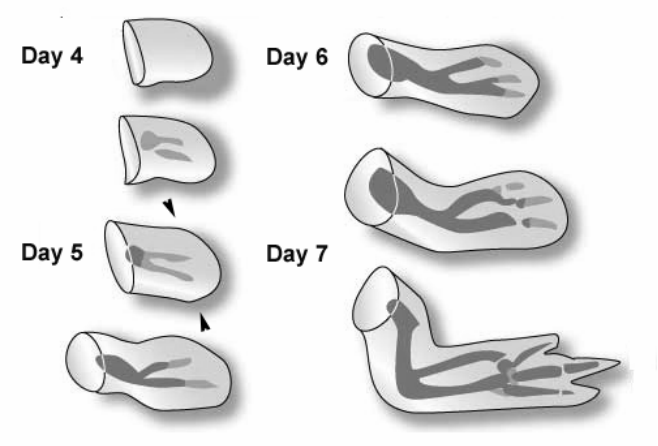
Day 4
Day 6
Day 5
Day 7

Fig. 1

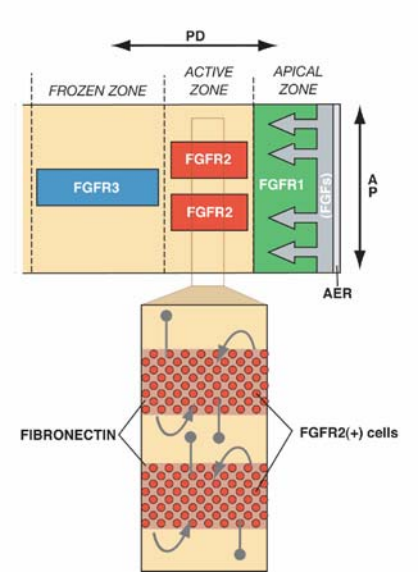
PD
FROZEN ZONE
ACTIVE ZONE
APICAL ZONE
FGFR3
FGFR2
FGFR2
FGFR1
(FGF)
AP
AER
FIBRONECTIN
FGFR2(+) cells

Fig. 2

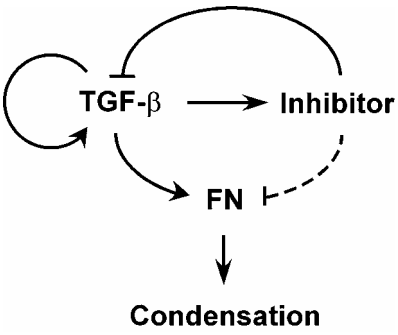

Fig. 3

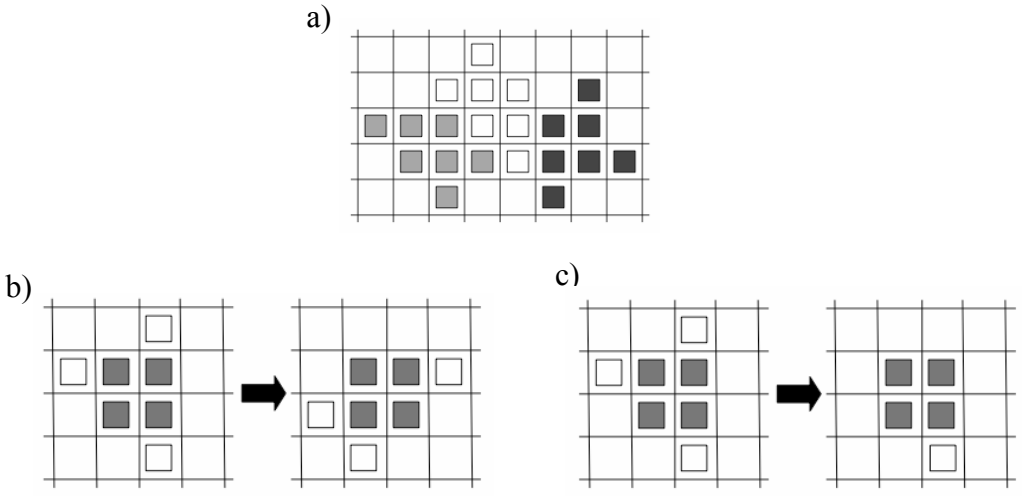

Fig. 4

A.

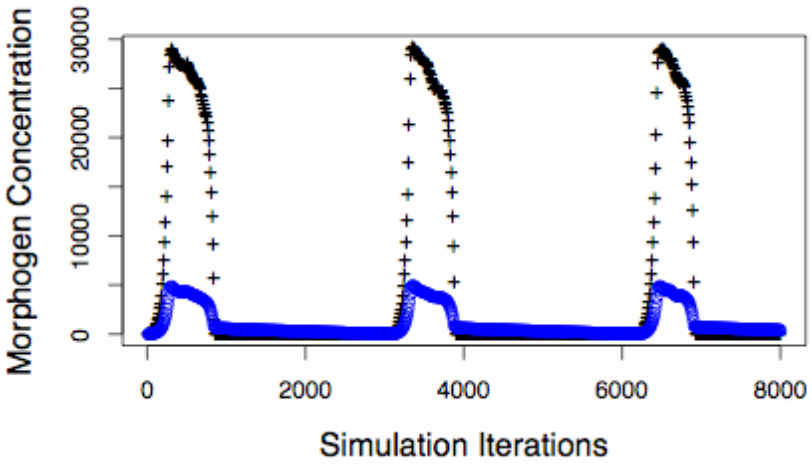
Morphogen Concentration
0
10000
20000
30000
0
2000
4000
6000
8000
Simulation Iterations

B.

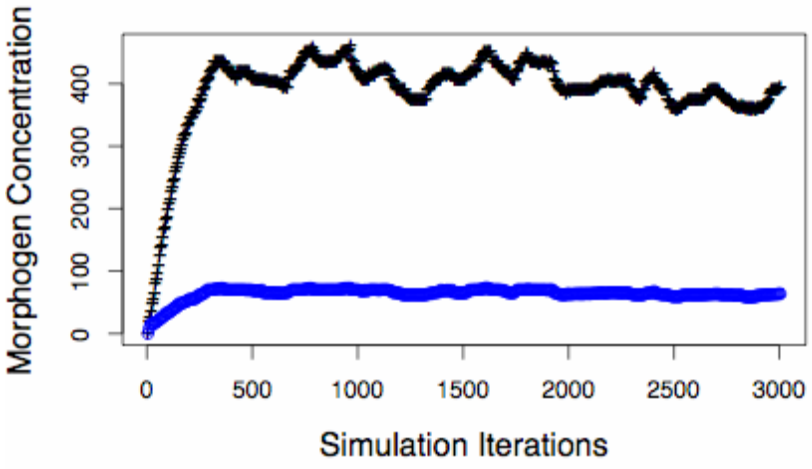
Morphogen Concentration
0
100
200
300
400
0
500
1000
1500
2000
2500
3000
Simulation Iterations

Fig. 5

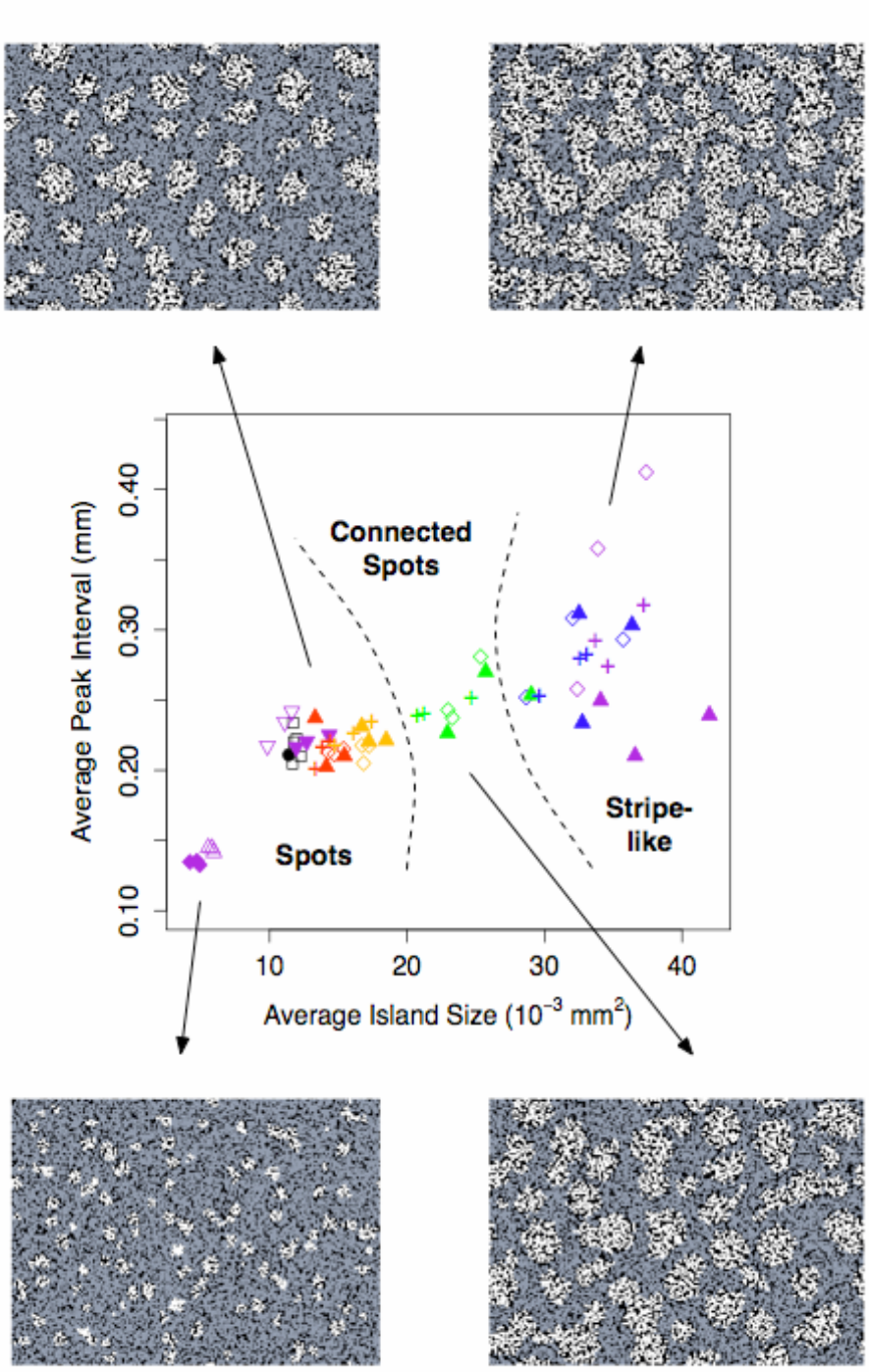
Connected Spots
Spots
Stripe-like
Average Peak Interval (mm)
0.10
0.20
0.30
0.40
10
20
30
40
Average Island Size (10^{-3} mm^2)

Fig. 6

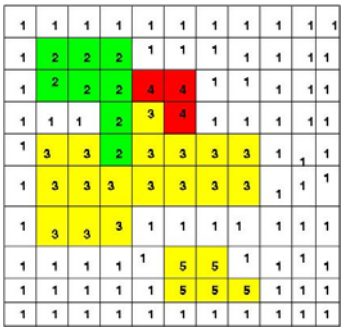

Fig. 7

(a) (b) (c)

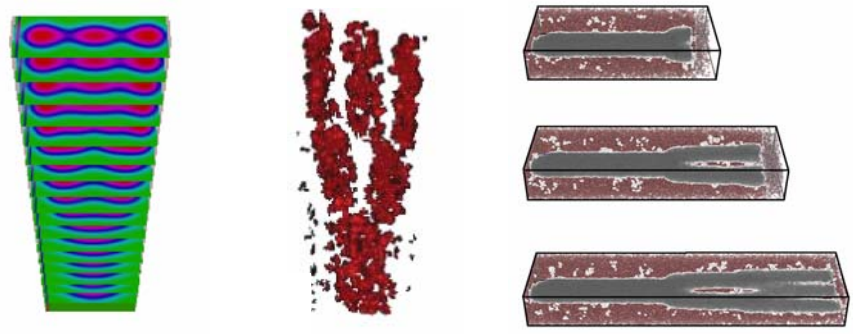

Fig. 8

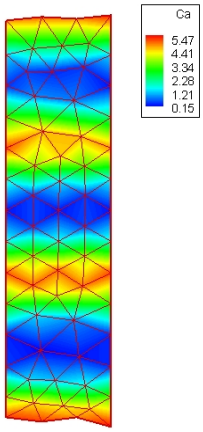
Ca
5.47
4.41
3.34
2.28
1.21
0.15

Fig. 9

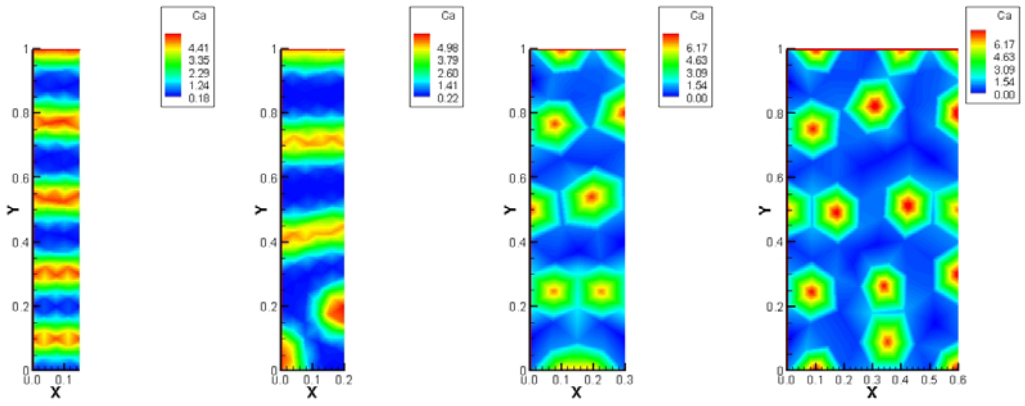
Ca
4.41
3.35
2.29
1.24
0.18
Ca
4.98
3.79
2.60
1.41
0.22
Ca
6.17
4.63
3.09
1.54
0.00
Ca
6.17
4.63
3.09
1.54
0.00
Y
X

Fig. 10